https://doi.org/10.52676/1729-7885-2025-4-127-141
УДК 544.6: 004.94: 620.9: 546.11: 538.9: 532.5

PHOTOELECTROCHEMICAL WATER SPLITTING SIMULATION: TOWARD A COMPREHENSIVE MODELING FRAMEWORK

N. Bakranov[1], B. Seitov[2], D. Bakranova[3*], E. Fattahi[4,5], A. Çoruh[4], A. Niaei[4]

[1] Research Group altAir Nanolab LLP, Almaty, Kazakhstan
[2] Ahmet Yassawi University, Turkestan, Kazakhstan
[3] SDU University, Faculty of Engineering & Natural Sciences, Kaskelen, Kazakhstan
[4] Department of Physics, Faculty of Science, Sakarya University, Sakarya, Turkey
[5] Department of Chemical Engineering, University of Tabriz, Tabriz, Iran

** E-mail for contacts: dinabakranova@gmail.com*

This study presents a comprehensive computational framework that integrates physics-based modeling and data-driven approaches for analyzing and optimizing photoelectrochemical (PEC) water splitting systems. Utilizing COMSOL Multiphysics 6.1 and MATLAB, we simulate key electrochemical behaviors such as linear sweep voltammetry (LSV) and electrochemical impedance spectroscopy (EIS). COMSOL's multiphysics environment allows for the direct incorporation of electrolyte parameters, semiconductor photophysics, and current distribution, while MATLAB enables custom modeling of impedance behavior and predictive LSV analysis using artificial neural networks (ANNs). By coupling computational fluid dynamics (CFD), machine learning, and experimental validation, the proposed methodology provides an in-depth understanding of light-driven hydrogen generation on semiconductor electrodes such as $ZnO/BiVO_4$. Comparative analysis of simulation results shows that COMSOL and MATLAB produce consistent outputs, yet COMSOL demonstrates superior flexibility, accuracy, and ease of use, especially for systems influenced by variable physical and chemical conditions. The study further explores two-phase flow modeling, mesh independence testing, and the influence of gas bubbles on electrolyte conductivity. The findings contribute to the development of efficient, scalable PEC systems for clean hydrogen production and offer a foundation for future integration of hybrid simulation and AI techniques in renewable energy research.

Keywords: *photoelectrochemical water splitting, COMSOL Multiphysics, MATLAB, electrochemical impedance spectroscopy, artificial neural networks, hydrogen production, electrochemical modeling.*

INTRODUCTION

The excessive use of fossil fuels has made it urgent to develop renewable and sustainable energy sources to address the challenges associated with the energy crisis. In terms of direct solar energy conversion and storage, hydrogen has garnered significant attention due to its high energy density (120–142 MJ/kg) and the potential to obtain it from water. When used as an energy carrier, hydrogen is highly efficient. It can be employed for transportation, storage, and power generation in areas where other energy sources are difficult or costly to access. Additionally, the fact that its combustion produces only water vapor makes hydrogen particularly appealing as a clean energy solution [1].

Photoelectrochemical (PEC) water splitting systems are a promising and sustainable method for producing green hydrogen by harnessing solar energy. PEC systems utilize semiconductor photoelectrodes to convert solar light into chemical energy, leading to the decomposition of water into hydrogen and oxygen. This approach offers a carbon-free and environmentally friendly pathway to meet future energy demands.

The photoelectrochemical (PEC) system operates based on several key principles. First, a semiconductor photoelectrode absorbs sunlight, where photons with energy equal to or greater than the bandgap excite electrons from the valence band to the conduction band, forming electron-hole pairs. These charge carriers must then be efficiently separated and transported: electrons typically migrate to the external circuit or the counter electrode, while holes remain in the photoelectrode. At the electrode–electrolyte interface, redox reactions occur – holes in the photoanode oxidize water molecules to produce oxygen gas, protons, and electrons. Meanwhile, the electrons travel to the cathode, where they reduce protons to form hydrogen gas. From an energetic perspective, the water-splitting reaction requires a minimum energy input of 1.23 eV; however, additional voltage, known as overpotential, is necessary to overcome kinetic barriers. For effective PEC operation, the band edges of the semiconductor must be appropriately aligned: the conduction band edge should lie at a more negative potential than the H^+/H_2 reduction level, while the valence band edge should be more positive than the O_2/H_2O oxidation potential (Figure 1).

An essential consideration in the operation of a photoelectrochemical (PEC) cell is the necessity of employing a potentiostat-galvanostat system. Indeed, its use is required to optimize PEC water splitting performance. Illumination by sunlight or artificial light sources is used to excite the semiconductor photoanode, generating electron-hole pairs that facilitate the water-splitting reactions. In contrast, electrolysis performed solely with a potentiostat in the absence of illumination constitutes conven-

tional electrolysis, which generally demands higher electrical energy input. The integration of solar illumination with an applied external bias significantly lowers the total electrical energy required, thus improving the overall energy efficiency and sustainability of the process. Unlike traditional electrolysis, which depends entirely on electrical power, PEC systems leverage both photonic and electrical inputs, enabling lower operational voltages. While solar energy or lamp-based illumination primarily drives the photoelectrode activity, the application of an external potential – commonly controlled via a potentiostat – remains essential in both experimental and practical PEC water splitting to enhance charge separation, reaction kinetics, and hydrogen evolution efficiency [3, 4].

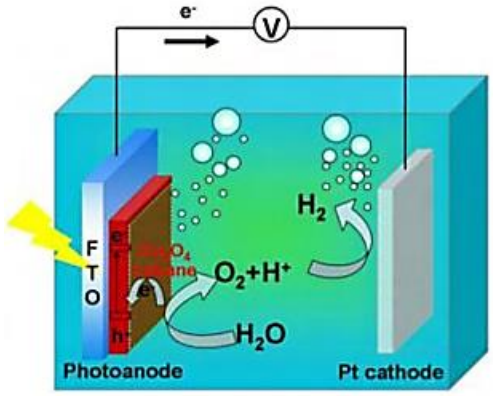

Figure 1. Schematic of a PEC system [2]

In recent years, various semiconductors such as TiO_2, ZnO, SiC, α-Fe_2O_3, WO_3, and $BiVO_4$ have been proposed and extensively studied as photoanodes. Their wide application is attributed to a combination of availability, high stability, and environmental safety. Among these materials, $BiVO_4$ has attracted particular attention due to its relatively narrow band gap (~2.4 eV), which enables efficient light absorption and photogeneration of charge carriers [5]. $BiVO_4$ is an n-type semiconductor with a band gap of 2.4 eV and can serve as a non-toxic photoanode active in the visible range. The favorable alignment of its band edges with the redox potentials of water makes $BiVO_4$ a promising candidate not only for PEC water splitting (Figure 2) but also for CO_2 reduction systems. The theoretical solar-to-hydrogen (STH) efficiency of $BiVO_4$ reaches 9.1%, creating strong expectations for its future commercialization [6]. However, the performance of $BiVO_4$-based photoanodes remains limited by the sluggish kinetics of the oxygen evolution reaction (OER). This limitation is caused by the high kinetic barrier of water oxidation and severe surface recombination of charge carriers due to their poor mobility [7]. As a result, the photocurrent density of $BiVO_4$-based systems rarely approaches the theoretical maximum of 7.5 mA·cm^{-2} at 1.23 V vs RHE.

To enhance activity, various strategies have been explored, including controlled growth of specific crystallographic facets, defect engineering, formation of oxygen vacancies, and doping with metals or non-metals to tune the electronic properties of $BiVO_4$. Considerable attention has been given to the development of highly active OER catalysts and interface engineering between the catalyst and $BiVO_4$ [8]. For example, the introduction of a hole transport layer can suppress interfacial recombination and improve system efficiency. Notably, the incorporation of Co_3O_4 nanoparticles between NiOOH and $BiVO_4$ results in the NiOOH/Co_3O_4/$BiVO_4$ photoanode, which delivers a photocurrent density of 6.4 mA·cm^{-2} at 1.23 V vs RHE with stability up to 90 h. The formation of p–n junctions with Co_3O_4 promotes efficient hole extraction and accelerates water oxidation, enabling charge separation efficiencies of 95.6% and charge transfer efficiencies of 97.7% [9]. Similarly, Fang et al. demonstrated that the deposition of NiFeOOH and Co-Pi cocatalysts increases the photocurrent to 2.03 mA·cm^{-2} at 1.23 V vs RHE, which is 5.8 times higher than that of pristine $BiVO_4$ [10].

Another promising approach to improving the photoelectrochemical activity of $BiVO_4$ is the construction of heterostructures. In Ag–Pi/$BiVO_4$ systems, the built-in electric field greatly accelerates hole transport and charge separation, while WO_3/$BiVO_4$ core–shell heterostructures compensate for the low carrier mobility of $BiVO_4$ and significantly enhance PEC performance.

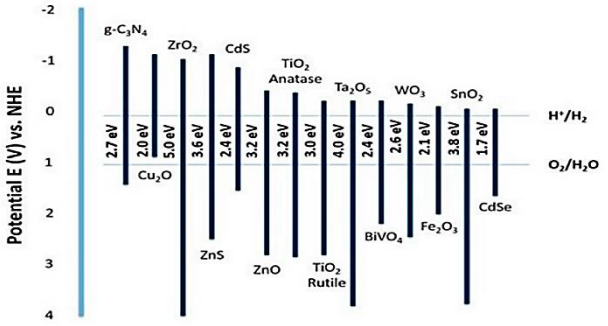

Figure 2. Band edge positions of typical semiconductors used for water splitting. Reproduced from [11] with permission from MDPI

Thus, the integration of semiconductors into heterostructures can mitigate the limitations of individual components and improve overall efficiency [12]. For instance, in the multilayer WO_3/$BiVO_4$/TiO_2 photoelectrode, $BiVO_4$ acts as the light absorber, TiO_2 serves as a protective layer against photocorrosion, and WO_3 functions as the conductive layer [13]. Since charge separation and transport directly determine the concentration of holes participating in oxidation reactions, the introduction of semiconductor layers onto $BiVO_4$ not only enhances light absorption but also forms heterojunctions that facilitate charge separation [14].

Beyond heterostructures, increasing attention has also been directed toward $BiVO_4$ homostructures formed by combining different crystalline forms of the same material. In particular, the combination of monocrystalline and polycrystalline $BiVO_4$ allows one to merge the

advantages of high carrier mobility in the single crystal with the large active surface area and facile synthesis of the polycrystal. Monocrystalline $BiVO_4$ exhibits much higher electron conductivity (12 $cm^2 \cdot V^{-1} \cdot s^{-1}$) and fewer grain boundaries, thereby reducing carrier recombination. However, single crystals suffer from limited active surface area and complex synthesis, which restricts their practical use. Thus, homostructures that combine monocrystalline and polycrystalline phases can minimize carrier losses while simultaneously increasing the number of active reaction centers. This approach offers new opportunities for improving both the stability and efficiency of PEC processes, making $BiVO_4$-based homostructures a highly promising direction for further optimization [15].

Overall, among the various semiconductor photoanodes investigated, $BiVO_4$ stands out as one of the most promising due to its narrow band gap, favorable band edge positions, and high theoretical STH efficiency. At the same time, its intrinsic drawbacks-low electron mobility, surface recombination, and slow water oxidation kinetics-make $BiVO_4$ a model system for the development and testing of advanced PEC enhancement strategies. In particular, the design of hetero- and homostructures, the application of cocatalysts, passivation layers, and interface engineering allow for a deeper understanding of charge transfer mechanisms and reveal universal principles for optimizing photoanode performance. These factors explain the choice of $BiVO_4$ as the central focus of the present study, aimed at identifying and systematizing approaches to improve its activity and stability, while building a foundation for the future commercialization of PEC technologies. These findings are in good agreement with recent reports on rhodium-modified perovskite oxides for enhanced OER activity [16].

MODELING AND SIMULATION PEC SYSTEM

Electroanalysis is a scientific study focused on the quantitative measurement of the composition or properties of chemical systems using electrochemical techniques. Common electroanalytical methods include cyclic voltammetry, linear sweep voltammetry, chronopotentiometry, and electrochemical impedance spectroscopy. These experiments can be performed in either static electrolyte solutions or in solutions that are subjected to forced fluid flow.

The primary objectives of electroanalytical modeling in COMSOL Multiphysics include the determination of both kinetic and thermodynamic parameters associated with electrochemical reactions occurring at electrode surfaces. These simulations provide insights into the fundamental behavior of the electrochemical interface under various conditions. Additionally, electroanalysis allows for the characterization of mass transport properties, facilitating the study of how electroactive species diffuse, migrate, or convect within the electrolyte. Furthermore, COMSOL enables the exploration of reaction mechanisms, offering a detailed understanding of the electrochemical pathways and the subsequent chemical reactivity of the species formed during these processes [17].

Using CFD offers enhanced accessibility and the opportunity to explore complex systems that may be challenging to assess experimentally. Recognizing these benefits, it is crucial to focus on developing CFD simulation approaches for PEC cells. Machine learning methodologies, including artificial neural networks (ANN), have the potential to enhance predictive accuracy and optimize the operational efficacy of alkaline water spitting by utilizing data-driven insights.

COMSOL Multiphysics offers distinct advantages over MATLAB in the field of electrochemical modeling, primarily due to its native support for coupled multiphysics simulations. Unlike MATLAB, where individual governing equations such as Nernst–Planck (ion transport), Navier–Stokes (fluid dynamics), Poisson (electrical potential), and Butler–Volmer (electrode kinetics) must be implemented separately and manually coupled, COMSOL provides an integrated environment that solves these equations simultaneously within a unified framework [18, 19]. The graphical user interface in COMSOL further facilitates the construction of complex geometries – such as porous electrodes or microfluidic channels – and automatically generates high-quality finite element meshes, eliminating the need for manual scripting or external meshing tools often required in MATLAB. Additionally, COMSOL includes a built-in, robust finite element solver with automatic mesh refinement and convergence control, whereas MATLAB users must assemble system matrices, impose boundary conditions, and ensure numerical stability manually unless employing specialized toolboxes. Widely recognized in both academia and industry, COMSOL has become the standard platform for solving coupled multiphysics problems, supported by extensive validation studies. While MATLAB remains a powerful tool for algorithm development, data analysis, and simplified one-dimensional models, it lacks out-of-the-box capabilities for full-scale, three-dimensional multiphysics simulations.

In modeling the LSV curve using MATLAB coding, we define the Tafel or Butler-Volmer equation. However, in COMSOL, in addition to that information, we also need the concentration of the electrolyte and its conductivity, which are influential parameters in electrochemistry, especially in LSV curves. The COMSOL software is more comprehensive and includes all relevant details, whereas, in MATLAB, this is not the case. Another consideration is that when using ANN in the electrochemistry field, especially when training a LSV curve, a substantial amount of data is required. The more databases are applied in ANN modeling, the more accurate the network will be, and consequently, it will be able to predict other circumstances. In contrast, with the limited experimental data available, we will be able to train it and use it for predictions in COMSOL.

Experimental Studies on $ZnO/BiVO_4$ -based PEC Water Splitting Systems are summarized in Table 1.

Simulation and modeling studies in PEC water splitting are further summarized in Table 2.

Table 1. Experimental Studies on $ZnO/BiVO_4$ -based PEC Water Splitting Systems

№	Electrodes Used	PEC Performance	Ref.
1	Photoanode: $ZnO/BiVO_4$ on ITO Counter: Pt Ref: Ag/AgCl	J = 1.72 mA/cm^2 @ 1.2 V vs Ag/AgCl	[20]
2	Photoanode: a thin film of $BiFeO_3$ nanosheets on FTO Counter: Pt Ref: Ag/AgCl	0.56 μA cm^{-2} under continuous light illumination, and 0.07 μA cm^{-2} In the absence of light.	[21]
3	Photoanode: $ZnO/BiVO_4$/Co-Pi Counter: Pt	Onset = 0.09 V_RHE; J = 3.4 mA/cm^2 @ 0.6 V_RHE	[22]
4	Photoanode: $ZnO/BiVO_4$/NiFePB Counter: Pt	J = 1.66 mA/cm^2 @ 1.23 V_RHE	[23]
5	Photoanode: $WO_3/BiVO_4$/Co-Pi; Counter: Pt	J = 6.7 mA/cm^2 @ 1.23 V_RHE	[24]
6	Photoanode: $BiVO_4$; Counter: Pt	solar-to-hydrogen (STH) efficiency is around 5% for single $BiVO_4$ photoanodes and >8% for tandem systems.	[25]
7	Photoanode: $BiVO_4$/FeOOH Counter: Pt	J ≈ 1 mA/cm^2 @ 0.6 V_RHE	[26]
8	Photoanode: $ZnO/BiVO_4$ Counter: Pt	The Co-Pi/$BiVO_4$/ZnO nano dendrite array photoanode achieved 3.5 mAcm^{-2} at 1.23 V vs. RHE, demonstrating improved performance compared to bare $BiVO_4$.	[27]
9	Photoanode: $BiVO_4$/Mo Counter: Pt	STH up to ~3% in prototype	[28]
11	Photoanode: $BiVO_4$/ $NiFeO_x$ Counter: Pt	The hydrogenated $BiVO_4$ photoanodes, when coupled with a $NiFeO_x$ cocatalyst, achieve a high efficiency of 1.91% at 0.58 V vs RHE.	[29]
13	Photoanode: $BiVO_4$; Counter: Pt		[30]

Table 2. Simulation and modeling studies on PEC water splitting system

№	Modeling/simulation Method	Software	Key results	Ref.
1	ANN prediction	MATLAB + ANN	Photocurrent prediction and system tuning	[31]
2	Carrier transport modeling	COMSOL	Charge separation efficiency	[32]
3	Nernst–Planck & Butler–Volmer equation	COMSOL	Design validation– Improved solar-to-hydrogen conversion efficiency	[33]
4	FEM ion transport	-	Potential and current distribution	[34]
5	Modeling of charge transfer	MATLAB	Photo absorber J–V, mass + charge transport	[35]
6	light absorption and charge separation	COMSOL	photocatalytic performance	[36]
7	Electrochemical kinetics at electrode/electrolyte interface	COMSOL	Overpotentials and catalytic activity	[37]

The present study aims to establish a comprehensive modeling and simulation framework for photoelectrochemical (PEC) water splitting systems, with a focus on analyzing and optimizing their electrochemical performance. Two primary simulation platforms are employed in this work: COMSOL Multiphysics 6.1 and MATLAB. COMSOL is utilized to perform linear sweep voltammetry (LSV) simulations under varying operational conditions to evaluate the photoelectrode activity, as well as electrochemical impedance spectroscopy (EIS) analyses to investigate charge-transfer mechanisms and interfacial properties. In parallel, MATLAB is used to implement artificial neural networks (ANNs) for predicting LSV behavior, allowing a comparative evaluation of ANN predictions against COMSOL-based results. Additionally, MATLAB-based custom code is developed for modeling impedance spectra, providing an alternative route to validate and interpret electrochemical data. By integrating physics-based simulations with data-driven approaches, the study seeks to gain deeper insight into PEC system behavior, assess the accuracy and reliability of different modeling techniques, and support future experimental validation.

Ultimately, this integrated approach enhances the understanding of PEC hydrogen production systems and contributes to the development of efficient and scalable clean energy technologies.

As mentioned earlier, at the beginning of the project, we also modeled impedance in both software to compare their accuracy. After that, we used the Tafel equation to model the kinetics of electrochemical reactions in both software to highlight the software of COMSOL and its superiority in application. In the following, the process of coupling the neural network and COMSOL with the electrolysis of water with graphite electrodes was also carried out.

METHODOLOGY

Methodology for Simulating Impedance of Randles Circuit:

In MATLAB:

1) Define circuit parameters: R_s (solution resistance), R_{ct} (charge transfer resistance), C_{dl} (double-layer capacitance), ω (angular frequency $2\pi f$), j (imaginary unit $\sqrt{-1}$).

2) Generate logarithmic frequency vector

3) Calculate total impedance using the modeled Randles model formula (1).

4) Plot Nyquist diagram (real vs. imaginary impedance)

$$z(\omega) = R_s + \frac{1}{\left(\frac{1}{R_{ct}} + j\omega C_{dl}\right)}. \quad (1)$$

In COMSOL Multiphysics:

EIS was simulated using the Electroanalysis physics interface in COMSOL Multiphysics. A small sinusoidal perturbation was applied to the working electrode potential, and the resulting current response was recorded. The impedance was calculated over a logarithmic frequency range. Material properties, electrode kinetics (via the Butler–Volmer equation), and double-layer capacitance were defined based on literature values. The Nyquist plot was then generated using the simulation results.

Methodology of modeling Tafel equation in MATLAB and COMSOL:

In the MATLAB section, we will define the Tafel equation using code. For comparison with COMSOL software, we will select the secondary current distribution physics and choose the electrode reaction equation known as the Tafel equation.

Methodology for Coupling COMSOL and ANN:

Figure 3 depicts the modeling procedures suggested in this study. The initial phase involved CFD simulation, encompassing the precise design of the system's geometry, the modeling of the electrochemical and momentum sections, and the meshing process. Following validation of the outcomes to confirm their accuracy, the subsequent step involved creating a dataset derived from the simulation results that reflected the influence of operational parameters, such as temperature and electrolyte concentration. This dataset was then imported into the neural network toolbox within MATLAB.

An ANN was employed to model and predict the current density (J) based on three input parameters: potential (V), temperature (T), and concentration (C). MATLAB was used as the computational platform to implement, train, and validate the ANN. ANN generally consists of three main layers: input, hidden, and output. In Figure 4, the ANN developed in this study is illustrated, showcasing layers of interconnected neurons. The outputs are derived from computations executed by the neurons from the preceding layer. The ANN modeling process consists of testing, training, and validation. Unlike other training algorithms, the Levenberg–Marquardt training algorithm demonstrated superior performance, leading to its selection for training this ANN model. The 2008 datasets generated by CFD modeling in COMSOL Multiphysics were classified into three distinct categories, namely, 70% for training (1406 datasets), 15% for testing (301 datasets), and 15% reserved for validation (301 datasets). They were exported to MATLAB for the development of the ANN model.

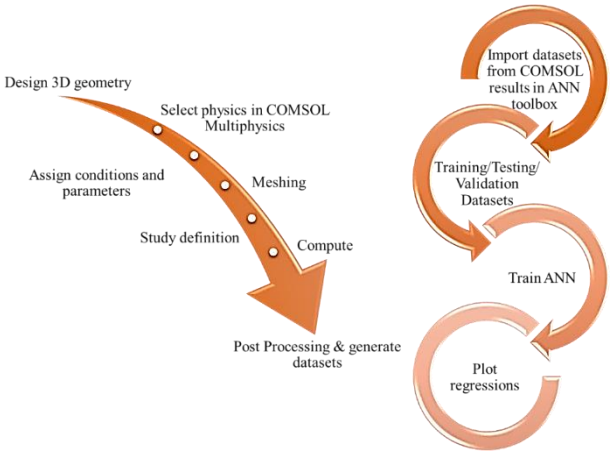

Figure 3. The sequence of executing the steps of the suggested modeling in methodology

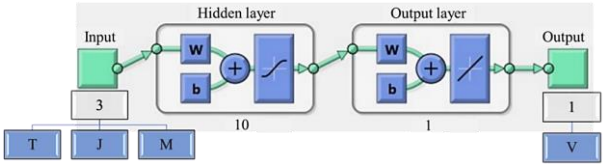

Figure 4. Schematic representation of the proposed artificial neural network

The accuracy of the COMSOL simulation against experimental data was evaluated by calculating the coefficient of determination (R^2), as illustrated in equation (2) [38]:

$$R^2 = 1 - \frac{\sum_{i=1}^{n}\left(y_{i,\exp} - y_{i,CFD}\right)^2}{\sum_{i=1}^{n}\left(y_{i,\exp} - \overline{y_{i,\exp}}\right)^2}. \quad (2)$$

Ion conductivity in electrolytes adheres to Ohm's law (3) and (4), which states that the electric current flowing through a conductor is directly related to the voltage difference between its terminals [39]. The electrolyte's conductivity is ascertained through equation (5). Equation (6) modifies the electrical conductivity of the electrolyte by accounting for the bubbles generated at the electrodes. These bubbles act like resistance and reduce the conductivity of the electrolyte [40, 41]. The Tafel equation (a simplified version of the Butler-Volmer equation due to overpotentials exceeding 100 mV of electrodes [42]) models the current density at the electrode surfaces, as outlined in equation (7) [43]. The energy efficiency of the

cell was calculated using the higher heating value (HHV) of hydrogen, referencing the thermoneutral voltage of 1.48 V, as presented in equation (8) [44–46]. Ultimately, the standard potential, U_{stn}, of the two-electrode cell is calculated through (9) as an operating temperature-dependent variable.

$$\nabla \cdot J = Q \rightarrow J = -\sigma \nabla \varnothing, \tag{3}$$

$$\nabla \cdot i = Q_j, \tag{4}$$

$$\sigma_0 = -204.1M - 0.28M^2 + 0.5332MT + \\ +20720\frac{M}{T} + 0.1043M^3 - 0.00003M^2T^2, \tag{5}$$

$$\sigma_{real} = \sigma_0 \left(1-\varepsilon\right)^{1.5}, \tag{6}$$

$$\eta = b \cdot \log\left(\frac{J}{J_0}\right), \tag{7}$$

$$\eta = \frac{1.48}{\varnothing}, \tag{8}$$

$$U_{stn} = 1.5184 - 1.5421 \cdot 10^{-3} \cdot T + \\ +9.523 \cdot 10^{-5} \cdot T \cdot \ln T + 9.84 \cdot 10^{-8} \cdot T^2. \tag{9}$$

In this system, it was observed that the bubbles generated on the electrode surface do not detach from it. Therefore, the effect of gas generation was effectively accounted for as a decrease in electrolyte conductivity. These adherent gas bubbles preserve the electrolyte's single-phase status. Nevertheless, we employed the Euler-Euler Model and Laminar Flow physics to investigate the dispersed phase of the produced bubbles within a two-phase system. The results showed that the volume fraction of the bubbles is zero (data will be provided in the next part). Given the certainty of the system's single-phase nature, as confirmed by experimental observations and computational results, we model the system under this condition.

The electrolyte phase is considered a Creeping Flow due to its complete immobility. The modified Navier-Stokes and continuity equations characterize the dynamics of velocity and pressure within the electrolyte phase [47]. The inertial term (Stokes flow) was neglected as a modification of the Navier-Stokes equation (10) and (11). Table 1 lists the parameters used to model the 3D two-electrode AWE setup.

$$0 = -\nabla P + \rho g + \nabla K, \tag{10}$$

$$\rho \nabla \cdot V = 0. \tag{11}$$

The physics of secondary current distribution and creeping flow were selected in the COMSOL Multiphysics® software along with a steady-state study, for modeling.

Figure 5 illustrates the geometrical configuration developed for the system using COMSOL Multiphysics 6.1® software. This geometric design was derived from the experimental setup employed to assess the GR performance and confirm the accuracy of the simulation findings.

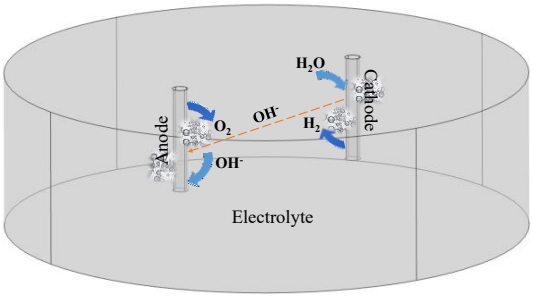

Figure 5. The system geometry in COMSOL Multiphysics® software.

Two phase flow modeling

The Euler-Euler model was used to model two-phase flow. Firstly, the model calculates the volume fraction of the continuous and the dispersed phases using the continuity equation, as shown in equations (12) and (13) [39]:

$$\frac{\partial}{\partial t}\left(\rho_c \phi_c\right) + \nabla \cdot \left(\rho_c \phi_c u_c\right) = m_{dc}, \tag{12}$$

$$\frac{\partial}{\partial t}\left(\rho_d \phi_d\right) + \nabla \cdot \left(\rho_d \phi_d u_d\right) = -m_{dc}, \tag{13}$$

where ϕ shows the volume fraction of each phase (dimensionless), u is the velocity (m/s), ρ is the density (kg/m^3), and m_{dc} is the mass transfer rate from the dispersed to the continuous phase (kg/(s·m^3)). The subscripts c and d represent the continuous and dispersed phases, respectively.

Equation (14) describes the relationship between the volume components of two phases. The continuity equation for the mixture is given by (15) [39].

$$\phi_c = 1 - \phi_d, \tag{14}$$

$$\nabla \cdot \left(\phi_d u_d + u_c\left(1-\phi_d\right)\right) = m_{dc}\left(\frac{1}{\rho_c} - \frac{1}{\rho_d}\right). \tag{15}$$

The momentum balance equation for the continuous phase and dispersed phase is expressed as follows [39]:

$$\rho_c \phi_c \left[\frac{\partial}{\partial t}\left(u_c\right) + u_c \nabla \cdot \left(u_c\right)\right] = -\phi_c \nabla P + \phi_c \nabla \cdot \tau_c + \\ +\phi_c \rho_c g + F_{m,c} + \phi_c F_c + m_{dc}\left(u_{\text{int}} - u_c\right), \tag{16}$$

$$\rho_d \phi_d \left[\frac{\partial}{\partial t}\left(u_d\right) + u_d \nabla \cdot \left(u_d\right)\right] = -\phi_d \nabla P + \phi_d \nabla \cdot \tau_d + \\ +\phi_d \rho_d g + F_{m,d} + \phi_d F_d - m_{dc}\left(u_{\text{int}} - u_d\right), \tag{17}$$

in which, P – represents the pressure of the mixture (Pa), g – denotes gravitational acceleration (m/s^2), u_{int} – signifies interphase velocity (m/s), τ – is the viscous stress tensor (Pa), – F_m indicates interphase momentum transfer (N/m^3), and F refers to any other volume force (N/m^3).

In multiphase flow systems, the drag force is considered the most important interphase force [48], and the following equation is used to calculate it [39]:

$$F_{m,c} = -F_{m,d} = \frac{3}{4d_d}\phi_c\phi_d C_D \rho_c \left|u_{slip}\right| u_{slip}\,. \quad (18)$$

In (18), d_d represents the diameter of the dispersed particles (m), and C_D is the drag coefficient. Slip velocity is defined as:

$$u_{slip} = u_d - u_c\,. \quad (19)$$

C_D is calculated using the Schiller-Naumann relation (20). The particle Reynolds number, Re_p, is determined using (21) [39]:

$$C_D = \begin{cases} \dfrac{24}{\mathrm{Re}_p}\left(1 + 0.15\,\mathrm{Re}_p^{0.687}\right) & \mathrm{Re}_p < 1000 \\ 0.44 & \mathrm{Re}_p \geq 1000 \end{cases} \quad (20)$$

$$\mathrm{Re}_p = \frac{d_d \rho_c \left|u_{slip}\right|}{\mu_c}\,. \quad (21)$$

Bubble dispersion is included in the momentum equation using a volume force according to [49]:

$$F_{BD} = -\phi_d \rho_c \frac{K_g}{d_d}\left|u_{slip}\right| \nabla \varnothing_d\,, \quad (22)$$

where K_g/d_b is the gas-phase dispersion factor, which is 5 m/s for oxygen and 2.5 m/s for hydrogen.

The viscous stress tensors are calculated according to the following relations [50]:

$$\tau_c = \mu_c\left(\nabla u_c + \left(\nabla u_c\right)^T - \frac{2}{3}\left(\nabla \cdot u_c\right) I\right), \quad (23)$$

$$\tau_d = \mu_d\left(\nabla u_d + \left(\nabla u_d\right)^T - \frac{2}{3}\left(\nabla \cdot u_d\right) I\right). \quad (24)$$

Lastly, the Faradaic equation calculates the amount of hydrogen and oxygen gas produced (g/(m^2·s)) by the reaction on the electrode surface, as a function of the electrode's current density (25) and (26). To calculate the total amount of gas in each of the cathode and anode chambers, the amount of water vapor was taken into account (27–30) [39–51]:

$$m_{H2} = \frac{M_{H2}}{2F} \cdot i\,, \quad (25)$$

$$m_{O_2} = \frac{M_{O_2}}{4F} \cdot i\,, \quad (26)$$

$$P_{vapor} = 0.61121 \cdot \exp\left[\left(18.678 - \frac{T - 0\left[\deg C\right]}{234.5\left[K\right]}\right) \cdot \left(\frac{T - 0\left[\deg C\right]}{257.14 + T - 0\left[\deg C\right]}\right)\right], \quad (27)$$

$$x_{H2O} = \frac{P_{vapor}}{p}\,, \quad (28)$$

$$m_{vap,cathode} = \frac{M_{H_2O}}{2F} \cdot i \cdot \frac{x_{H_2O}}{1 - x_{H_2O}}\,, \quad (29)$$

$$m_{vap,anode} = \frac{M_{H_2O}}{4F} \cdot i \cdot \frac{x_{H_2O}}{1 - x_{H_2O}}\,, \quad (30)$$

where M_{H_2}, M_{H_2O}, and M_{O_2} are the molecular weights of hydrogen, water, and oxygen. P_{vapor} is the water vapor pressure, P is the operating pressure, which is standard pressure (1 atm), T is the operating temperature in °C, and x_{H_2O} is the mole fraction of water vapor in the gas phase.

PEC water splitting simulation

PEC water splitting systems rely on the interplay between photogenerated charge carriers and electrochemical redox reactions at the semiconductor–electrolyte interface. In contrast to conventional water electrolysis, which requires a minimum thermodynamic potential of 1.23 V under standard conditions, PEC systems can achieve water splitting at significantly lower applied voltages. This is because incident photons excite electrons from the valence band to the conduction band of a semiconductor, generating electron-hole pairs that contribute part of the Gibbs free energy required for water splitting. As a result, the external bias needed to drive the redox reactions is reduced, effectively lowering the onset potential of the system. This photovoltage, generated internally by the light-absorbing semiconductor, plays a crucial role in enabling spontaneous or low-bias-driven water splitting reactions. Therefore, light not only activates the semiconductor but also alters the electrochemical potential landscape at the interface, tightly coupling photo- and electrochemical processes.

In this simulation, we employ a hybrid modeling approach to capture both the photophysical behavior of the semiconductor photoelectrode and the electrochemical reactions at the semiconductor–electrolyte interface. The model combines two physics interfaces in COMSOL Multiphysics: Semiconductor (under illumination) and Secondary Current Distribution.

First, semiconductor physics is used to simulate light absorption and carrier transport within the photoelectrode. Generation of electron–hole pairs due to incident light is defined through an optical generation term, and the internal electric potential is computed by solving the coupled Poisson and drift–diffusion equations. The resulting electrostatic potential at the interface between the semiconductor and electrolyte represents the photovoltage developed due to illumination.

Next, this photovoltage is used as an input into the Secondary Current Distribution interface to model the electrochemical kinetics. The potential difference between the semiconductor surface and the reversible water-splitting potential (1.23 V vs. RHE) is used to define

the local overpotential driving the reaction. The Butler–Volmer equation is applied at the interface to describe the charge transfer between the photoelectrode and the electrolyte.

This approach allows for the analysis of how illumination affects the onset potential and current density in PEC water splitting, effectively linking the semiconductor's photogenerated potential to the electrochemical performance of the system.

RESULTS

Comparison of EIS outcomes acquired from two mathematical approaches

At the beginning of the results section, we attempted to model the Nyquist plot using both COMSOL and MATLAB. In MATLAB, we wrote code to obtain the results, while in COMSOL, we used the Electroanalysis physics module. Figure 6 presents the EIS results for a pre-prepared sample from the experimental setup, COMSOL simulation, and MATLAB modeling. As shown, MATLAB and COMSOL demonstrate similar capabilities in predicting the Nyquist plot of the sample. Compared to the experimental data, both simulations exhibit some deviation and are not entirely accurate. Nevertheless, our primary focus is on the similarity in their prediction abilities. COMSOL, with its user-friendly interface and predefined equations, provides a comparable level of accuracy to MATLAB, which requires more extensive coding efforts.

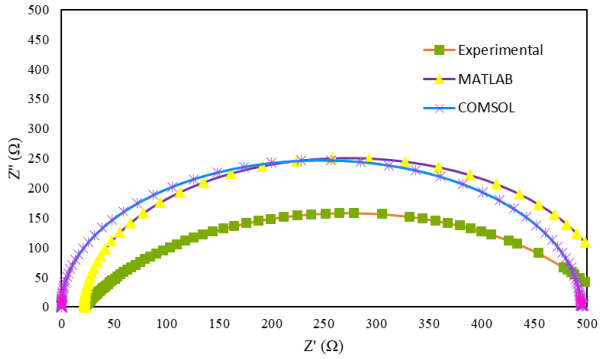

Figure 6. Nyquist plot obtained from experimental test, COSMOL simulation, and MATLAB modeling

This code was developed to simulate the impedance behavior of a water electrolysis system. experimental impedance curve presented in Figure 6 was obtained from one of our synthesized perovskite oxides ($LaFeO_3$) under dark water electrolysis conditions. This data was utilized exclusively for extracting the electrochemical parameters listed in Table 3 and for validating the numerical implementation of the COMSOL–MATLAB model ensuring accurate representation of the electrochemical behavior in the simulations. Under illumination, the charge transfer resistance (R_{ct}) decreases due to increased generation of charge carriers and enhanced electrochemical reaction rates. Therefore, for a PEC cell, we simply replace the R_{ct} value with the new, illumination-dependent value to account for the effect of light on the system's impedance.

In photoelectrochemical (PEC) water splitting, illumination plays a critical role in determining the electrochemical behavior of the system. Two important parameters used to characterize this effect are the light sensitivity coefficient (k) and the normalized light intensity (I). The light sensitivity coefficient is a dimensionless quantity that reflects the extent to which the electrochemical response of the PEC cell varies with changes in illumination. Higher values of k indicate greater sensitivity to light intensity fluctuations. The normalized light intensity I represents the ratio of the applied light intensity to a standard reference, typically taken as the AM 1.5G solar spectrum at 1000 W/m^2. This normalization allows for consistent comparison of PEC performance under different experimental or simulated lighting conditions, using a scale ranging from 0 (complete darkness) to 1 (standard full illumination). Despite the utility of these parameters, a universally applicable equation describing the precise dependence of electrochemical behavior on k and I has yet to be established, due to the complexity and variability of PEC systems.

However, in practice, especially for systems with a fixed and well-defined light source (such as ours), these settings are unnecessary. Because the light intensity remains constant throughout testing, there is no need to model variations in lighting. The impedance modeling including the equivalent circuit and governing equations, in PEC water splitting compared to water electrolysis, is intact. The sole modification being the illumination-adjusted values of electrochemical parameters, The only thing that changes is the charge transfer resistance R_{ct}, which is determined by the system under certain lighting circumstances. Thus, there is no need to include or change k, I, or the corresponding equations during simulations. This method simplifies modeling while properly describing the system's behavior under constant light.

Table 3 provides the details of the parameters inserted into MATLAB and COMSOL software to obtain the Nyquist plot.

Table 3. The details of the parameters inserted into MATLAB and COMSOL software

Parameter	Symbol	Unit	Value
Solution Resistance	R_s	Ω	21.77
Charge Transfer Resistance	R_{ct}	Ω	501.1
Double-Layer Capacitance	C_{dl}	F	$6.3 \cdot 10^{-4}$
High frequency	f_{max}	Hz	100000
Low frequency	f_{min}	Hz	0.01

Comparing LSV curves obtained from coding in MATLAB and simulation through COMSOL

It is evident from the results in Figure 7 that both mathematical approaches – COMSOL simulation and MATLAB coding – yield nearly identical results. Nonetheless, a significant differentiation emerges when scrutinizing the influence of electrolyte concentration on electrocatalytic efficacy. While MATLAB coding, which is based on the classical Tafel equation, does not

incorporate an explicit parameter for electrolyte concentration, COMSOL facilitates the direct integration of electrolyte concentration as an input variable that significantly affects the LSV characteristics. The classical Tafel equation does not explicitly account for electrolyte concentration as a variable; hence, its impact can only be integrated empirically through MATLAB by adjusting the exchange current density J_0, which necessitates extensive and dependable experimental data. This constraint diminishes the model's precision and increases reliance on numerous experiments to calibrate the parameters accurately.

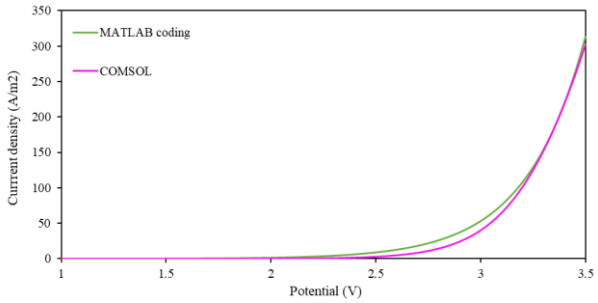

Figure 7. Comparing LSV curves obtained from coding in MATLAB and simulation through COMSOL

Alternatively, the effect of electrolyte concentration on mass transport can be modeled by introducing a limiting current density that depends on the concentration. However, the modeling of the limiting current density entails a considerable simplification: it presumes a uniform concentration field and disregards spatial variations, convective transport, and the effects of electrode geometry. This approximation may result in considerable inaccuracies in practical systems. It should also be noted whether there is a limiting current density in the system. In the perovskite materials we have investigated, no limiting current density has been observed in the potential ranges tested so far.

Table 4. The details of the parameters inserted into MATLAB and COMSOL software to obtain the LSV curve

Parameter	Symbol	Unit	Value
Tafel slope	b	V/dec	0.282
Equilibrium potential	E_{eq}	V	1.23
Applied potential range	E	V	1–3.5
Exchange current density	I_0	A/m^2	0.1

In contrast, COMSOL Multiphysics offers a comprehensive simulation environment that enables the direct input of physical and chemical properties, including electrolyte concentration. Without modifying the fundamental governing equations, one can quickly and accurately investigate the effect of electrolyte concentration on electrocatalyst performance by simply adjusting this parameter. This flexibility significantly reduces the time and cost of experimentation and analysis while enhancing confidence in the simulation results. Table 4 provides the details of the parameters inserted into MATLAB and COMSOL software to obtain the LSV curve.

Coupling COMSOL and ANN

Initially, the electrocatalytic performance of GR toward OER and HER was evaluated in a three-electrode setup to determine its electrochemical parameters, J_0 and b. Polarization curves under operating conditions of 25 °C and 70 °C are illustrated in Figure 8a and 8b. Subsequently, the Arrhenius diagram was plotted based on the exchange current density and temperature, allowing for the determination of J_0 without requiring further laboratory testing. This diagram can be used to predict J_0 at any temperature, as shown in Figures 8c and 8d. The slope of the Arrhenius plot exhibits values of −1556 and −602.1 for the OER and the HER curves, respectively.

The current density measured at 0 V vs. RHE was observed to be negative, with the cathodic current onset shifted toward more negative potentials. This phenomenon can be attributed to several well-established factors [52–54]. Firstly, graphite electrodes are known to catalyze oxygen reduction at low potentials due to the presence of dissolved O_2, leading to the emergence of cathodic current even prior to the thermodynamic onset of the hydrogen evolution reaction (HER). Secondly, potential cycling during electrode conditioning may result in the activation of the graphite surface by introducing edge sites, structural defects, or partial oxidation. These modifications enhance the electrode's catalytic behavior and can shift the HER onset to more positive potentials. Additionally, graphite exhibits a relatively high double-layer capacitance, and capacitive (non-Faradaic) currents may contribute significantly to the background signal, particularly at low scan rates. To mitigate these effects, it is advisable to degas the electrolyte with N_2 or Ar prior to measurements and to minimize potential cycling when using freshly prepared electrodes.

Moreover, graphite demonstrates a markedly higher exchange current density (J_0) for the oxygen evolution reaction (OER) compared to HER, which can be explained by several material-specific properties [55–59]. Under anodic polarization, the graphite surface becomes enriched with oxygen-containing functional groups that increase its activity toward OER. In contrast, HER requires efficient hydrogen adsorption and fast electron transfer – conditions for which graphite is inherently less favorable due to its poor hydrogen binding characteristics. Furthermore, elevated temperatures and anodic potentials promote oxidative modifications on the graphite surface, generating reactive sites conducive to OER, while offering limited benefit to HER kinetics.

In summary, the higher j_0 observed for OER on graphite compared to HER reflects graphite's relatively better catalytic activity for OER due to the formation of active oxygen species on its surface and its inherent limitations in hydrogen adsorption. This is consistent with experimental findings and supports the understanding that graphite is a more efficient catalyst for OER than for HER.

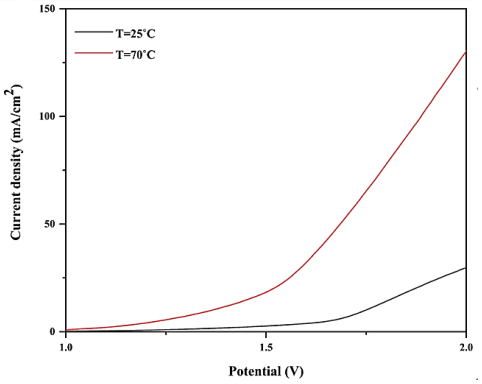

a)

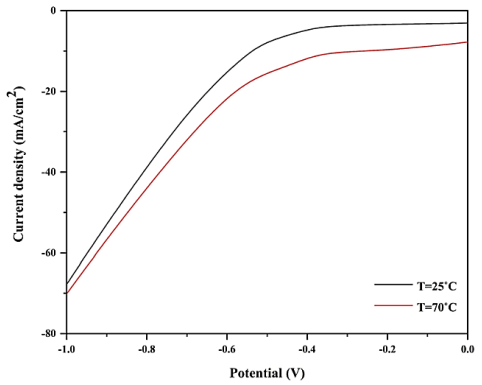

b)

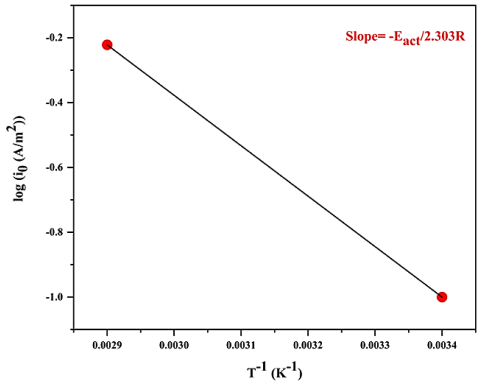

c)

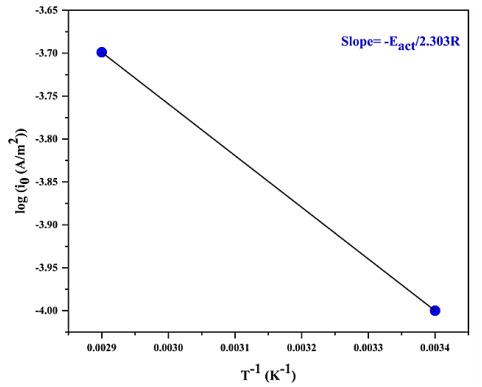

d)

Figure 8. OER polarization curve (a), HER polarization curve (b), Arrhenius plot as anode (c), and Arrhenius plot as cathode (d) of the GR electrode

Checking mesh independence is one of the most essential steps in any simulation [60]. The non-dependence of the solution on the meshing should be checked in all simulation software that divides the computational domain into smaller sub-domains. Examining mesh independence involves selecting the optimal mesh to obtain accurate results. In this work, an independence test was conducted on the meshing results to determine the optimal meshing of the system. The number of elements in the Normal, Coarse, and Coarser meshes was 87,307, 66,808, and 24,655, respectively. Coarse meshing yields the most accurate results with the most optimized runtime and memory usage (Figure 9a).

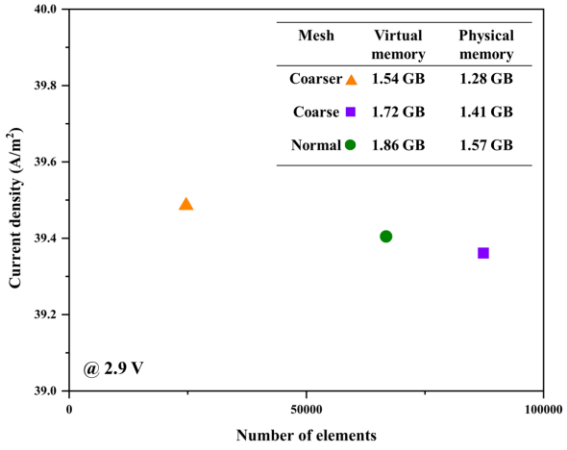

a)

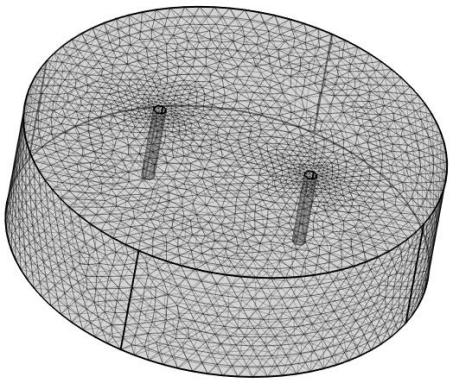

b)

Figure 9. The current density @ 2.9 V in the different element numbers, the physical and virtual memory used (a) and Coarse system meshing (b)

The relative change between Coarse and Normal meshes was only 0.11%, indicating negligible variation [61]. Therefore, Coarse meshing was used in this work (Figure 9b).

Two phase flow results

We had previously observed during experimental tests that bubbles produced on the electrode surface do not separate from them and therefore do not enter the electrolyte phase, but instead act as a resistor. However, we attempted to model the system as a two-phase system,

so that after verifying whether the system is single-phase or two-phase, we could proceed with modeling it.

The bottom image shows the volume fraction of bubbles in the system, which we observe to be zero (Figure 10a). Figure 10b also indicates the electrolyte velocity distribution. The electrolyte in our experimental system remains stationary due to the absence of inflow or outflow, as well as the lack of electrolyte injection in the middle or RDE system, which would create movement within the electrolyte. The modeling results show a minimal value for the electrolyte velocity, which is confirmed to be correct. The stationary nature of the electrolyte is one of the reasons it remains single-phase, as the completely stationary phase prevents bubbles from moving.

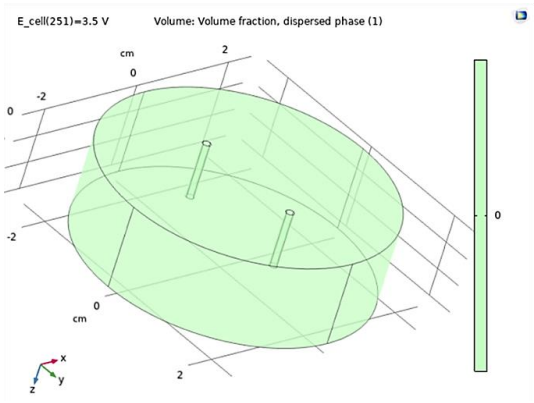

a)

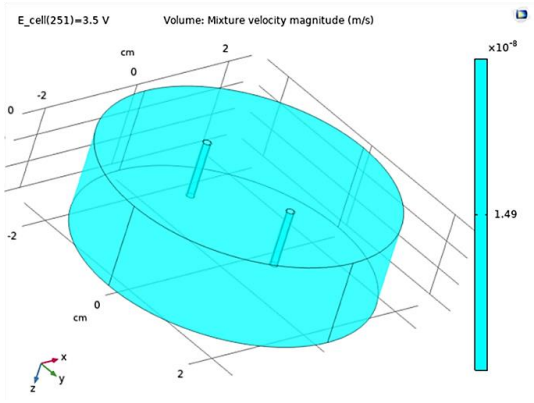

b)

Figure 10. Volume fraction (a) and electrolyte phase velocity (b)

CONCLUSION

In this work, we developed and validated a hybrid modeling framework to simulate photoelectrochemical water splitting using both COMSOL Multiphysics and MATLAB environments. Through a series of simulations and ANN-based predictions, we demonstrated that both platforms can effectively model electrochemical processes such as impedance behavior and current–voltage characteristics. However, COMSOL proved to be more comprehensive and efficient, particularly due to its built-in multiphysics solvers, flexible geometry handling, and direct parameter integration, such as electrolyte concentration, which is otherwise challenging to account for in MATLAB without extensive experimental data.

Moreover, we showed that coupling COMSOL simulations with machine learning tools in MATLAB (ANN) enables predictive modeling with high accuracy, thereby reducing the experimental workload. The inclusion of two-phase flow simulations confirmed the single-phase behavior of the system under stationary electrolyte conditions, with negligible bubble motion and volume fraction. Mesh independence testing further ensured the reliability and efficiency of the computational model.

This integrated approach not only enhances our understanding of PEC hydrogen production mechanisms but also contributes to the advancement of simulation techniques in electrochemical energy systems. Nevertheless, a limitation of this study is the absence of experimental validation; while the simulations provide valuable insights, their predictive reliability remains constrained without corresponding experimental confirmation. Future work will focus on extending the model to include new photoelectrode materials, implementing real-time data feedback into ANN models, and conducting in-depth experimental validations under variable light and electrolyte conditions to further optimize system performance for industrial application.

Acknowledgments

During the preparation of this work the authors used ChatGPT (Version 4.0) to improve the English language of this manuscript. All content was subsequently reviewed and edited by the authors, who take full responsibility for the final version of the publication.

Declaration of Competing Interest

The authors declare that the research was conducted in the absence of any commercial or financial relationships that could be construed as a potential conflict of interest.

Funding information

The author(s) declare that financial support was received for the research, authorship, and/or publication of this article. This research has been funded by the Science Committee of the Ministry of High Education and Science of the Republic of Kazakhstan (Grant No. AP23490626 "Research and development of ZnO/$BiVO_4$ and Cu_2O/ZnO photoelectrodes to create highly efficient tandem light-driven hydrogen production systems").

REFERENCES

1. Hosseini S.E, Wahid M.A. Hydrogen production from renewable and sustainable energy resources: Promising green energy carrier for clean development // Renewable and Sustainable Energy Reviews. – 2016. – Vol. 57. – Issue C. – P. 850–866. https://doi.org/10.1016/j.rser.2015.12.112

2. Ma P., Wang D. The principle of photoelectrochemical water splitting. Nanomaterials for Energy Conversion and Storage // World Scientific. – 2018. – Vol. 1. – P. 61.
3. Zhang H., Zhang B., Wang X., Zou L., You J., Lin S. Effective charge separation in photoelectrochemical water splitting: A review from advanced evaluation methods to materials design // Sustain Energy Fuels. – 2024.
4. Ager J.W. Photoelectrochemical approach for water splitting // Solar to Chemical Energy Conversion: Theory and Application. – 2016. – Vol. 249. – P. 60.
5. Feng S., et al. Using hollow dodecahedral NiCo-LDH with multi-active sites to modify $BiVO_4$ photoanode facilitates the photoelectrochemical water splitting performance // Nano Research Energy. – 2024. – Vol. 3(3).
6. Mane P., et al. Recent trends and outlooks on engineering of $BiVO_4$ photoanodes toward efficient photoelectrochemical water splitting and CO_2 reduction: A comprehensive review // Int. J. of Hydrogen Energy. – 2022. – Vol. 47(94). – P. 39796–39828.
7. Sung H., et al. Dense/nanoporous bilayer $BiVO_4$ photoanode with outstanding light-absorption efficiency for high-performance photoelectrochemical water splitting // J. of Photochemistry and Photobiology A-Chemistry. – 2024. – P. 449.
8. Fu L., Li Z, and Shang X. Recent surficial modification strategies on $BiVO_4$ based photoanodes for photoelectrochemical water splitting enhancement // Int. J. of Hydrogen Energy. – 2024. – Vol. 55. – P. 611–624.
9. Zhang Y., et al. Engineering $BiVO_4$ and Oxygen Evolution Cocatalyst Interfaces with Rapid Hole Extraction for Photoelectrochemical Water Splitting // Acs Catalysis. – 2023. – Vol. 13(9). – P. 5938–5948.
10. Fang G., Liu Z., and Han C. Enhancing the PEC water splitting performance of $BiVO_4$ co-modifying with NiFeOOH and Co-Pi double layer cocatalysts // Applied Surface Science. – 2020. – Vol. 515.
11. Shabdan Y., et al. Photoactive Tungsten-Oxide Nanomaterials for Water-Splitting // Nanomaterials. – 2020. – Vol. 10(9).
12. Yin D., et al. Dual modification of $BiVO_4$ photoanode for synergistically boosting photoelectrochemical water splitting // J. of Colloid and Interface Science. – 2023. – Vol. 646. – P. 238–244.
13. Kyaw A., et al. Fabrication and characterization of heterostructure WO_3/$BiVO_4$/TiO_2 photocatalyst for efficient performance of photoelectrochemical water splitting // Current Applied Physics. – 2025. – Vol. 72. – P. 87–92.
14. Wang L., et al. Recent advances in elaborate interface regulation of $BiVO_4$ photoanode for photoelectrochemical water splitting // Materials Reports: Energy. – 2023. – Vol. 3(4).
15. Teh I., et al. Engineering high-performance $BiVO_4$ homo- and heterojunction Photoanodes for solar-driven Photoelectrochemical water splitting applications // Coordination Chemistry Reviews. – 2025. – Vol. 541. – P. 216773.
16. G.A. Kaptagay, B.M. Satanova, A.U. Abuova, M. Konuhova, Zh.Ye. Zakiyeva, U.Zh Tolegen, N.O. Koilyk, F.U. Abuova, Effect of rhodium doping for photocatalytic activity of barium titanate // Optical Materials: X. – 2025. – Vol. 25. – P. 100382.
17. COMSOL Multiphysics, Electrochemistry Module User's Guide, version 5.4, Chapter 3: Electrochemistry Interfaces, COMSOL AB n.d.; 1998–2023, p. 60.
18. Idoko I.P., Ezeamii G.C., Idogho C., Peter E., Obot U.S., Iguoba V.A. Mathematical modeling and simulations using software like MATLAB, COMSOL and Python // Magna Scientia Advanced Research and Reviews. – 2024. – Vol. 12. – P. 62–95.
19. Dickinson E.J.F., Ekström H., Fontes E. COMSOL Multiphysics®: Finite element software for electrochemical analysis. A mini-review // Electrochem Commun. – 2014. – Vol. 40. – P. 71–74.
20. Bera S., Ghosh S., Shyamal S., Bhattacharya C., Basu R.N. Photocatalytic hydrogen generation using gold decorated $BiFeO_3$ heterostructures as an efficient catalyst under visible light irradiation // Solar Energy Materials and Solar Cells. – 2019. – Vol. 194. – P. 195–206.
21. Yan L., Zhao W., Liu Z. 1D ZnO/$BiVO_4$ heterojunction photoanodes for efficient photoelectrochemical water splitting // Dalton Transactions. – 2016. – Vol. 45. – P. 11346–11352.
22. Kim K., Moon J.H. Three-dimensional bicontinuous $BiVO_4$/ZnO photoanodes for high solar water-splitting performance at low bias potential // ACS Appl Mater Interfaces. – 2018. – Vol. 10. – P. 34238–34244.
23. Bai S., Jia S., Zhao Y., Feng Y., Luo R., Li D., et al. NiFePB-modified ZnO/$BiVO_4$ photoanode for PEC water oxidation // Dalton Transactions. – 2023. – Vol. 52. – P. 5760–5770.
24. Pihosh Y., Turkevych I., Mawatari K., Uemura J., Kazoe Y., Kosar S., et al. Photocatalytic generation of hydrogen by core-shell WO_3/$BiVO_4$ nanorods with ultimate water splitting efficiency // Sci. Rep. – 2015. – Vol. 5. – P. 11141.
25. Yin X., Yang X., Qiu W., Wang K., Li W., Liu Y., et al. Boosting the photoelectrochemical performance of $BiVO_4$ photoanodes by modulating bulk and interfacial charge transfer // ACS Appl. Electron Mater. – 2021. – Vol. 3. – P. 1896–1903.
26. Kim T.W., Choi K-S.. Nanoporous $BiVO_4$ photoanodes with dual-layer oxygen evolution catalysts for solar water splitting // Science (1979). – 2014. – Vol. 343. – P. 990–994.
27. Yang J-S., Wu J-J.. Low-potential driven fully-depleted $BiVO_4$/ZnO heterojunction nanodendrite array photoanodes for photoelectrochemical water splitting // Nano Energy. – 2017. – Vol. 32. – P. 232–240.
28. Tolod K.R., Hernández S., Russo N. Recent advances in the $BiVO_4$ photocatalyst for sun-driven water oxidation: top-performing photoanodes and scale-up challenges // Catalysts. – 2017. – Vol. 7. – P. 13.
29. Wu H., Zhang L., Qu S., Du A., Tang J., Ng Y.H. Polaron-mediated transport in $BiVO_4$ photoanodes for solar water oxidation // ACS Energy Lett. – 2023. – Vol. 8. – P. 2177–2184.
30. Vilanova A., Dias P., Lopes T., Mendes A. The route for commercial photoelectrochemical water splitting: a review of large-area devices and key upscaling challenges // Chem. Soc. Rev. – 2024. – Vol. 53. – P. 2388–2434.
31. Diaby M., Alimi A., Bardaoui A., Santos D.M.F., Chtourou R., Ben Assaker I. Correlation between the experimental and theoretical photoelectrochemical response of a WO_3 electrode for efficient water splitting through the implementation of an artificial neural network // Sustainability. – 2023. – Vol. 15. – P. 11751.
32. Huang H., Obata K., Kishimoto F., Takanabe K. Numerical modeling investigations of the impact of a thin p-type

cocatalyst modifier on an n-type photon absorber for unbiased overall solar water splitting // Mater. Adv. – 2022. – Vol. 3. – P. 9009–9018.
33. Njoka F.N., Ahmed M.A., Ookawara S. Design of a novel photoelectrochemical reactor for hydrogen production // Energy and Sustainability VII. – 2017. – Vol. 224. – P. 349.
34. Haussener S., Hu S., Xiang C., Weber A.Z., Lewis N.S. Simulations of the irradiation and temperature dependence of the efficiency of tandem photoelectrochemical water-splitting systems // Energy Environ. Sci. – 2013. – Vol. 6. – P. 3605–3618.
35. Chen Y. Numerical Simulation of Performance and Solar-To-Fuel Conversion Efficiency for Photoelectrochemical Devices // California Institute of Technology. – 2021.
36. Cendula P., Schumacher J.O. Spectroscopic modeling of photoelectrochemical water splitting. COMSOL Conference, Munich, Germany, 12-14 October 2016, COMSOL Group. – 2016.
37. Haussener S., Xiang C., Spurgeon J.M., Ardo S., Lewis N.S., Weber A.Z. Modeling, simulation, and design criteria for photoelectrochemical water-splitting systems // Energy Environ. Sci. – 2012. – Vol. 5. – P. 9922–9935.
38. Dhalsamant K. Development, validation, and comparison of FE modeling and ANN model for mixed-mode solar drying of potato cylinders // J. Food Sci. – 2021. – Vol. 86. – P. 3384–3402.
39. Yang W., Sun L., Tang J., Mo Z., Liu H., Du M., et al. Multiphase fluid dynamics and mass transport modeling in a porous electrode toward hydrogen evolution reaction // Ind. Eng. Chem. Res. – 2022. – Vol. 61. – P. 8323–8332.
40. Caspersen M., Kirkegaard J.B. Modelling electrolyte conductivity in a water electrolyzer cell // Int. J. Hydrogen Energy. – 2012. – Vol. 37. – P. 7436–7441.
41. Gilliam R.J, Graydon J.W, Kirk D.W, Thorpe S.J. A review of specific conductivities of potassium hydroxide solutions for various concentrations and temperatures // Int. J. Hydrogen Energy. – 2007. – Vol. 32. – P. 359–364.
42. Alom M.S., Kananke-Gamage C.C.W., Ramezanipour F. Perovskite oxides as electrocatalysts for hydrogen evolution reaction // ACS Omega. – 2022. – Vol. 7. – P. 7444–7451.
43. Rodríguez J., Amores E. CFD modeling and experimental validation of an alkaline water electrolysis cell for hydrogen production // Processes. – 2020. – Vol. 8. – P. 1634.
44. Li W., Tian H., Ma L., Wang Y., Liu X., Gao X. Low-temperature water electrolysis: fundamentals, progress, and new strategies // Mater. Adv. – 2022. – Vol. 3. – P. 5598–5644.
45. Lamy C., Millet P. A critical review on the definitions used to calculate the energy efficiency coefficients of water electrolysis cells working under near ambient temperature conditions // J. Power Sources. – 2020. – Vol. 447. – P. 227350.
46. Lettenmeier P. Efficiency–electrolysis. Siemens Energy Global GmbH Co KG, München, Germany, White Paper 2021.
47. Doering C.R., Gibbon J.D. Applied analysis of the Navier-Stokes equations. Cambridge university press, 1995.
48. Chen W, Zhang L. Effects of interphase forces on multiphase flow and bubble distribution in continuous casting strands // Metallurgical and Materials Transactions B. – 2021. – Vol. 52. – P. 528–547.
49. Le Bideau D., Mandin P., Benbouzid M., Kim M., Sellier M., Ganci F., et al. Eulerian two-fluid model of alkaline water electrolysis for hydrogen production // Energies (Basel). – 2020. – Vol. 13. – P. 3394.
50. Enwald H., Peirano E., Almstedt A-E. Eulerian two-phase flow theory applied to fluidization // International Journal of Multiphase Flow. – 1996. – Vol. 22. – P. 21–66.
51. Romagnuolo L., Yang R., Frosina E., Rizzoni G., Andreozzi A., Senatore A. Physical modeling of evaporative emission control system in gasoline fueled automobiles: A review // Renewable and Sustainable Energy Reviews. – 2019. – Vol. 116. – P. 109462.
52. Ricke N.D., Murray A.T., Shepherd J.J., Welborn M.G., Fukushima T., Van Voorhis T., et al. Molecular-level insights into oxygen reduction catalysis by graphite-conjugated active sites // ACS Catal. – 2017. – Vol. 7. – P. 7680–7687.
53. Gerischer H. An interpretation of the double layer capacity of graphite electrodes in relation to the density of states at the Fermi level // J. Phys. Chem. – 1985. – Vol. 89. – P. 4249–4251.
54. Allen B.W., Piantadosi C.A. Electrochemical activation of electrodes for amperometric detection of nitric oxide // Nitric Oxide. – 2003. – Vol. 8. – P. 243–252.
55. Rahimian M., Ghaffarinejad A., Arabi M. Water splitting by electrodepositing Ni–Co on graphite rod: Low-cost, durable, and binder-free electrocatalyst // Int. J. Hydrogen Energy. – 2024. – Vol. 81. – P. 852–864.
56. Lipka S.M., Cahen Jr G.L., Stoner G.E., Scribner Jr L.L, Gileadi E. Hydrogen and oxygen evolution on graphite fiber –epoxy matrix composite electrodes // Electrochim. Acta. – 1988. – Vol. 33. – P. 753–760.
57. Chhetri M., Sultan S., Rao C.N.R.. Electrocatalytic hydrogen evolution reaction activity comparable to platinum exhibited by the Ni/Ni (OH) 2/graphite electrode // Proceedings of the National Academy of Sciences. – 2017. – Vol. 114. – P. 8986–8990.
58. Ficca V.C.A., Santoro C., Placidi E., Arciprete F., Serov A., Atanassov P., et al. Exchange current density as an effective descriptor of poisoning of active sites in platinum group metal-free electrocatalysts for oxygen reduction reaction // ACS Catal. – 2023. – Vol. 13. – P. 2162–2175.
59. Danaee I., Noori S. Kinetics of the hydrogen evolution reaction on NiMn graphite modified electrode // Int. J. Hydrogen Energy. – 2011. – Vol. 36. – P. 12102–12111.
60. Sadrehaghighi I. Mesh Sensitivity & Mesh Independence Study. CFD Open Series: Annapolis, MD, USA. – 2021. – P. 56.
61. Lee M., Park G., Park C., Kim C. Improvement of grid independence test for computational fluid dynamics model of building based on grid resolution // Advances in Civil Engineering. – 2020, – Vol. 2020. – P. 8827936.

СУДЫҢ ФОТОЭЛЕКТРОХИМИЯЛЫҚ ЫДЫРАУЫН МОДЕЛЬДЕУ: КЕШЕНДІ МОДЕЛЬДЕУ ЖҮЙЕСІН ҚҰРУ ЖОЛЫНДА

Н. Бакранов[1], Б. Сейтов[2], Д. Бакранова[3*], Е. Фаттахи[4,5], А. Чорух[4], А. Ниаеи[4]

[1] Research Group altAir Nanolab ЖШС, Алматы, Қазақстан
[2] Қожа Ахмет Ясауи атындағы Халықаралық қазақ-түрік университеті, Түркістан, Қазақстан
[3] SDU University, Инженерия және жаратылыстану ғылымдары факультеті, Қаскелең, Қазақстан
[4] Физика кафедрасы, Жаратылыстану ғылымдары факультеті, Сакария университеті, Сакария, Түркия
[5] Химиялық инженерия кафедрасы, Табриз университеті, Табриз, Иран

** Байланыс үшін E-mail: dinabakranova@gmail.com*

Бұл зерттеуде суды ыдыратын фотоэлектрохимиялық (ФЭХ) жүйелерді талдау және оңтайландыру үшін физикалық модельдеу мен деректерге негізделген тәсілдерді біріктіретін кешенді есептеу платформасы ұсынылған. COMSOL Multiphysics 6.1 және MATLAB көмегімен сызықтық вольтамперометрия (СВА) және электрохимиялық импеданс спектроскопиясы (ЭИС) сияқты негізгі электрохимиялық процестер модельденеді. COMSOL мультифизикалық ортасы электролит параметрлерін, жартылай өткізгіштердің фотофизикалық қасиеттерін және токтың таралуын тікелей есепке алуға мүмкіндік береді, ал MATLAB жасанды нейрондық желілерді (ЖНЖ) пайдалана отырып, реттелетін импеданс өзгерісін модельдеуді және СВА болжамды талдауын реттеуге мүмкіндік береді. Есептеу гидродинамикасының (ЕГД), машиналық оқытудың және эксперименттік тексерудің үйлесімі арқылы ұсынылған әдістеме $ZnO/BiVO_4$ сияқты жартылай өткізгіш электродтардағы жарықтың әсерінен сутектің пайда болу процесін терең түсінуге мүмкіндік береді. Модельдеу нәтижелерін салыстырмалы талдау COMSOL мен MATLAB үйлесімді нәтижелерді қамтамасыз ететінін көрсетті, COMSOL, әсіресе физикалық және химиялық жағдайлардың айнымалылары әсер ететін жүйелер үшін тамаша икемділікті, дәлдікті және пайдаланудың қарапайымдылығын көрсетеді. Зерттеу екі фазалы ағынды модельдеуді, торлардың тәуелсіздігін тексеруді және газ көпіршіктерінің электролит өткізгіштігіне әсерін одан әрі қарастырады. Нәтижелер таза сутекті өндіру үшін тиімді масштабталатын электрохимиялық синтез жүйелерін (РЕС) дамытуға ықпал етеді және гибридті модельдеу мен жасанды интеллект әдістерін жаңартылатын энергия көздерін зерттеуге болашақта біріктіруге негіз қалайды.

Түйін сөздер: *суды фотоэлектрохимиялық бөлу, COMSOL Multiphysics, MATLAB, электрохимиялық импеданс спектроскопиясы, жасанды нейрондық желілер, сутегі өндірісі, электрохимиялық модельдеу.*

МОДЕЛИРОВАНИЕ ФОТОЭЛЕКТРОХИМИЧЕСКОГО РАСЩЕПЛЕНИЯ ВОДЫ: НА ПУТИ К СОЗДАНИЮ КОМПЛЕКСНОЙ СИСТЕМЫ МОДЕЛИРОВАНИЯ

Н. Бакранов[1], Б. Сейтов[2], Д. Бакранова[3*], Е. Фаттахи[4,5], А. Чорух[4], А. Ниаеи[4]

[1] Research Group altAir Nanolab TOO, Алматы, Казахстан
[2] Международный казахско-турецкий университет имени Х.А. Ясави, Туркестан, Казахстан
[3] SDU University, Факультет инженерии и естественных наук, Каскелен, Казахстан
[4] Кафедра физики, факультет естественных наук, Университет Сакарья, Сакарья, Турция
[5] Кафедра химической инженерии, Тебризский университет, Тебриз, Иран

** E-mail для контактов: dinabakranova@gmail.com*

В данном исследовании представлена комплексная вычислительная платформа, объединяющая физическое моделирование и подходы, основанные на данных, для анализа и оптимизации фотоэлектрохимических (ФЭХ) систем разложения воды. Используя COMSOL Multiphysics 6.1 и MATLAB, моделируются ключевые электрохимические процессы, такие как линейная вольтамперометрия (ЛВА) и электрохимическая импедансная спектроскопия (ЭИС). Мультифизическая среда COMSOL позволяет напрямую учитывать параметры электролита, фотофизические свойства полупроводников и распределение тока, в то время как MATLAB позволяет настраивать пользовательское моделирование поведения импеданса и предиктивный анализ ЛВА с использованием искусственных нейронных сетей (ИНС). Благодаря сочетанию вычислительной гидродинамики (ВГД), машинного обучения и экспериментальной проверки предлагаемая методология обеспечивает глубокое понимание процесса генерации водорода под действием света на полупроводниковых электродах, таких как $ZnO/BiVO_4$. Сравнительный анализ результатов моделирования показывает, что COMSOL и MATLAB обеспечивают согласованные результаты, при этом COMSOL демонстрирует превосходную гибкость, точность и простоту использования, особенно для систем, подверженных влиянию переменных физических и химических условий. В исследовании дополнительно рассматриваются моделирование двухфазного потока, тестирование независимости сеток и влияние пузырьков газа на проводимость электролита. Полученные результаты способствуют разработке эффективных масштабируемых систем электрохимического синтеза (РЕС) для производства чистого водорода и закладывают основу для будущей интеграции гибридного моделирования и методов искусственного интеллекта в исследования возобновляемой энергетики.

Ключевые слова: *фотоэлектрохимическое расщепление воды, COMSOL Multiphysics, MATLAB, электрохимическая импедансная спектроскопия, искусственные нейронные сети, производство водорода, электрохимическое моделирование.*